Human Molecular Genetics, 2020, Vol. 29, No. 16 2708–2722

doi: 10.1093/hmg/ddaa160
Advance Access Publication Date: 27 July 2020
General Article

GENERAL ARTICLE

ROM1 contributes to phenotypic heterogeneity in PRPH2-associated retinal disease

Daniel Strayve[1,‡], Mustafa S. Makia[1,‡], Mashal Kakakhel[1], Haarthi Sakthivel[1], Shannon M. Conley[2,3], Muayyad R. Al-Ubaidi[1,4,5] and Muna I. Naash[1,4,5,*,†]

[1]Department of Biomedical Engineering, University of Houston, Houston, TX 77204, USA, [2]Department of Cell Biology, University of Oklahoma Health Sciences Center, Oklahoma City, OK 73104, USA, [3]Oklahoma Center for Neurosciences, University of Oklahoma Health Sciences Center, Oklahoma City, OK 73104, USA, [4]College of Optometry, University of Houston, Houston, TX 77004, USA and [5]Depatment of Biology and Biochemistry, University of Houston, Houston, TX 77204-5001, USA

*To whom correspondence should be addressed at: Department of Biomedical Engineering, University of Houston, 3517 Cullen Blvd., Room 2027, Houston, TX 77204-5060, USA. Tel: +1 713-743-1651; Fax: +1 713-743-0226; Email: mnaash@central.uh.edu

Abstract

Peripherin 2 (PRPH2) is a retina-specific tetraspanin protein essential for the formation of rod and cone photoreceptor outer segments (OS). Patients with mutations in *PRPH2* exhibit severe retinal degeneration characterized by vast inter- and intra-familial phenotypic heterogeneity. To help understand contributors to this within-mutation disease variability, we asked whether the PRPH2 binding partner rod OS membrane protein 1 (ROM1) could serve as a phenotypic modifier. We utilized knockin and transgenic mouse models to evaluate the structural, functional and biochemical effects of eliminating one allele of *Rom1* (*Rom1*$^{+/-}$) in three different *Prph2* models which mimic human disease: C213Y *Prph2* (*Prph2*$^{C/+}$), K153Del *Prph2* (*Prph2*$^{K/+}$) and R172W (*Prph2*^{R172W}). Reducing *Rom1* in the absence of Prph2 mutations (*Rom1*$^{+/-}$) had no effect on retinal structure or function. However, the effects of reducing *Rom1* in the presence of *Prph2* mutations were highly variable. *Prph2*$^{K/+}$/*Rom1*$^{+/-}$ mice had improved rod and cone function compared with *Prph2*$^{K/+}$ as well as amelioration of K153Del-associated defects in PRPH2/ROM1 oligomerization. In contrast, *Prph2*^{R172W}/*Rom1*$^{+/-}$ animals had worsened rod and cone function and exacerbated retinal degeneration compared with *Prph2*^{R172W} animals. Removing one allele of *Rom1* had no effect in *Prph2*$^{C/+}$. Combined, our findings support a role for non-pathogenic ROM1 null variants in contributing to phenotypic variability in mutant *PRPH2*-associated retinal degeneration. Since the effects of *Rom1* reduction are variable, our data suggest that this contribution is specific to the type of *Prph2* mutation.

Introduction

Peripherin 2 (PRPH2, also known as retinal degeneration slow/RDS) is a transmembrane structural glycoprotein with an integral role in the formation and structure of both rod and cone photoreceptor outer segments (OSs) (1,2). In the absence of PRPH2 photoreceptors do not form OSs (3) and in the presence of only one allele, photoreceptor structure and function are both significantly impaired (4). Mutations in *PRPH2* lead to a variety of autosomal dominant degenerative retinal diseases, such as retinitis pigmentosa and macular dystrophy and there are no

†Muna I. Naash, http://orcid.org/0000-0002-6534-5144
‡The authors wish it to be known that, in their opinion, the first two authors should be regarded as joint first authors.
Received: May 5, 2020. **Revised:** July 3, 2020. **Accepted:** July 16, 2020

established treatments for these blinding disorders (5). Critically, PRPH2-associated diseases exhibit a wide variety of intra- and inter-familial phenotypic heterogeneity (6–9).

PRPH2 function depends on the formation of several different types of oligomers, both homo-oligomers as well as hetero-oligomers with its binding partner rod OS membrane protein 1 (ROM1). Initially, PRPH2 and ROM1 assemble into non-covalently bound homo- and hetero-tetramers, and these tetrameric complexes further assemble via disulfide bonds mediated by C150 in PRPH2 and C153 in ROM1 (10–12). Covalently linked complexes take the form of homo- and hetero-octamers as well as larger PRPH2 homo-oligomers. Recent work has shown that non-covalently linked PRPH2/ROM1 complexes can initiate OS formation, but covalent oligomerization is crucial for proper OS maturation (13,14).

ROM1 is not as critical for OS structure and function as PRPH2. For example, photoreceptor structure and function is only modestly impaired in the *Rom1*$^{-/-}$ retina (15), and no pathogenic mutations in *ROM1* have been identified. However, substantial data from both patients and animal models suggest that ROM1 can contribute to or modify *PRPH2*-associated disease phenotypes. Digenic retinitis pigmentosa associated with PRPH2 and ROM1 mutations has been reported (16–18) and modeled in mice carrying the digenic *PRPH2* mutation L185P on the *Rom1*$^{+/-}$ background (19). In addition, the non-pathogenic ROM1 variant R229H led to worsened disease phenotypes in patients with R172W-PRPH2 associated macular dystrophy (20), and a family with retinitis pigmentosa in which there is a *ROM1* gene duplication (without known *PRPH2* mutations) has been reported (21). One of our overarching interests is to understand the causes of within-mutation phenotypic heterogeneity in *PRPH2*-associated disease, and this known information about *ROM1* makes it a strong candidate modifier gene.

To help evaluate the hypothesis that ROM1 can modify *PRPH2*-associated disease phenotypes, we evaluated the Y141C *Prph2* knockin mouse (22) in the presence/absence of ROM1 (23). Patients carrying the Y141C *PRPH2* mutation exhibit a high degree of intrafamilial disease heterogeneity with phenotypes ranging from retinitis pigmentosa to pattern and other macular dystrophies (24). The Y141C *Prph2* knockin mouse exhibits a cone-rod dystrophy phenotype characterized by more severe cone functional defects and the formation of abnormal PRPH2/ROM1 oligomers. Eliminating ROM1 in this model led to elimination of abnormal PRPH2/ROM1 complexes and conversion to a retinitis pigmentosa phenotype characterized by defects more severe in rods than cones and reductions in the total amount of PRPH2 present (23). These findings supported the idea that *ROM1* variants could contribute to *PRPH2*-associated heterogeneity. However, it is unclear whether the effects of eliminating *Rom1* would be similar with all *Prph2* mutants and whether the effects would require eliminating both *Rom1* alleles (i.e. *Rom1*$^{-/-}$), or whether removing a single *Rom1* allele (i.e. *Rom1*$^{+/-}$) would be sufficient to modify the *Prph2*-associated phenotype.

Here we undertook to address these questions. In the present study, we evaluate the effects of eliminating a *Rom1* allele in three additional previously characterized *Prph2* disease models; K153Del *Prph2*, C213Y *Prph2* and R172W *Prph2* (25–28). These three mutations exhibit different patient phenotypes. K153Del leads to retinitis pigmentosa, pattern dystrophy and fundus flavimaculatus (29); C213Y causes butterfly pattern dystrophy (30–32) and R172W leads to a macular dystrophy phenotype in which cones are most affected (20,33,34). Here, we report that removing one allele of *Rom1* from mice carrying these *Prph2* mutations does not have uniform effects, in one case improving, in a second case worsening, and in a third case not affecting *Prph2*-associated disease phenotypes. These striking findings fit well with the emerging body of literature on the role of *ROM1* as a contributor to *PRPH2*-associated phenotypic variability, and show that considering the contribution of *ROM1* to disease phenotype adds an additional layer of complexity to the already complex and multi-faceted disease mechanisms of *PRPH2*-associated disease.

Results

Structural and functional effects of *Rom1* ablation are not consistent across *Prph2* mutations

In our previous studies using the *Prph2* Y141C model, we observed that elimination of *Rom1* converted a phenotype that more severely affected cones to a phenotype that more severely affected rods (23). One of our major goals in this paper was to determine whether the effect of *Rom1* ablation was similar across multiple *Prph2* disease-causing mutants or was unique to Y141C. *PRPH2*-associated disease is autosomal dominant, so we crossed three of our *Prph2* mutants, K153Del knockin (*Prph2*$^{K/+}$), C213Y knockin (*Prph2*$^{C/+}$) and the R172W transgenic line (*Prph2*^{R172W}) (25,26,28) with *Rom1*$^{-/-}$ animals to generate *Prph2* heterozygotes on a *Rom1*$^{+/-}$ background. Due to breeding difficulties, *Prph2* heterozygotes on the *Rom1*$^{-/-}$ background were difficult to obtain so we largely limited our studies to the *Rom1*$^{+/-}$ background (and controls).

We first assessed rod and cone function via full-field electroretinography (ERG) under scotopic and photopic conditions. Removing one allele of *Rom1* (*Rom1*$^{+/-}$) had no significant effect on scotopic and photopic ERG function at either postnatal day (P) 30 or P90 (Fig. 1). We previously found that *Prph2*$^{K/+}$ animals exhibit rod and cone functional deficits compared with wild-type (WT) (25) and that finding was recapitulated here (Fig. 1). At P30 in the K153Del model, we observed significant improvement in rod function after removing one allele of *Rom1* (*Prph2*$^{K/+}$/*Rom1*$^{+/-}$ compared with *Prph2*$^{K/+}$) (Fig. 1C), a finding that was preserved at P90 (Fig. 1A and E). However, *Prph2*$^{K/+}$ animals exhibited similar scotopic ERG to *Prph2*$^{K/+}$/*Rom1*$^{-/-}$, suggesting that complete elimination of *Rom1* is not beneficial to rod function in the presence of the K153del mutation. At P30, cone function was not improved in the *Prph2*$^{K/+}$/*Rom1*$^{+/-}$ compared with *Prph2*$^{K/+}$ (Fig. 1D). However, at P90, cone function was significantly better in the *Prph2*$^{K/+}$/*Rom1*$^{+/-}$ compared with *Prph2*$^{K/+}$ (Fig. 1B and F), suggesting that ongoing cone loss of function was slower when one allele of *Rom1* was removed.

Removing *Rom1* had quite different effects on the ERG function in the R172W retina compared with the K153Del retina (representative traces in Fig. 2A and B). The *Prph2*^{R172W} exhibits early onset cone defects, with rod functional loss occurring later (Fig. 2 and (28)). At P30, scotopic ERG values were similar in the *Prph2*^{R172W} compared with *Prph1*^{R172W}/*Rom1*$^{+/-}$ and were only slightly reduced compared with WT and *Rom1*$^{+/-}$ (Fig. 2C). However, by P90, scotopic values were significantly worse in the *Prph2*^{R172W}/*Rom1*$^{+/-}$ compared with *Prph2*^{R172W} (Fig. 2A and E) suggesting that reducing ROM1 levels accelerated rod degeneration. Cone function was also slightly worsened by reducing ROM1 levels in the R172W (Fig. 2B). At P30, the reduction in photopic responses in *Prph2*^{R172W}/*Rom1*$^{+/-}$ compared with *Prph2*^{R172W} was statistically insignificant (Fig. 2D), but by P90, *Prph2*^{R172W}/*Rom1*$^{+/-}$ cone ERGs were significantly reduced compared with those in *Prph2*^{R172W} (Fig. 2F).

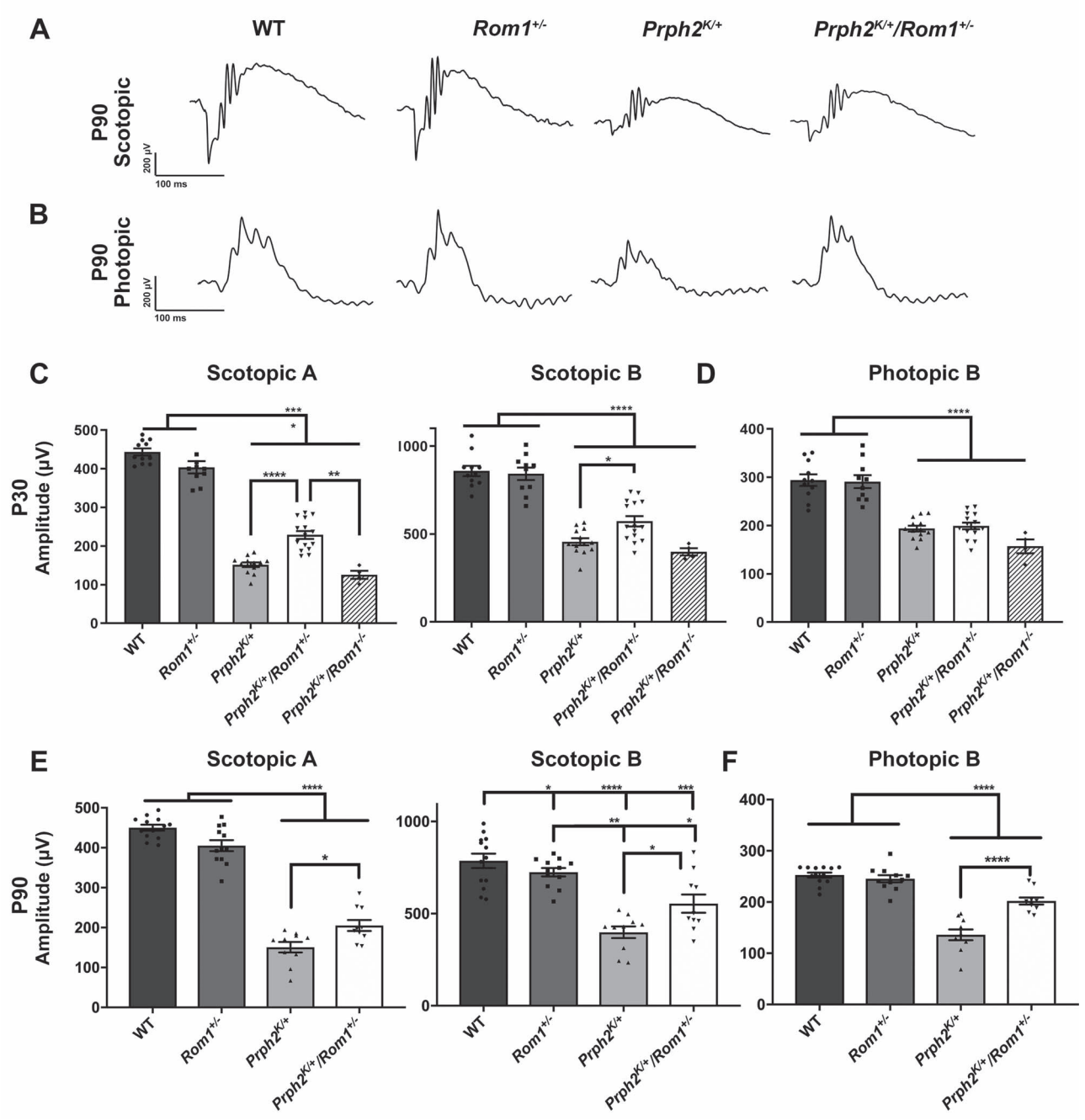

Figure 1. Partial ablation of *Rom1* improves rod and cone function in the *Prph2*$^{K/+}$. Full-field ERG was performed at P30 and P90. (**A-B**) Representative waveforms are shown from full-field ERGs collected at P90 under both scotopic (A) and photopic (B) conditions. (**C-E**) Plotted are mean ± SEM scotopic a- and b-wave at P30 (C) and P90 (E), and mean ± SEM photopic b-wave at P30 (D) and P90 (**F**). *$P < 0.05$, **$P < 0.01$, ***$P < 0.001$ by one-way ANOVA with Tukey's *post-hoc* comparison. $N = 10–15$ animals/genotype exception: $N = 4$ for *Prph2*$^{K/+}$/*Rom1*$^{-/-}$ (for reasons discussed in the text).

The effects of removing one allele of *Rom1* in the C213Y model were much smaller than in the previous two models (Fig. 3). The *Prph2*$^{C/+}$ retina exhibits early onset rod loss with more modest cone loss (Fig. 3 and (26)). At both P30 and P90, there was no significant difference in scotopic ERG function between *Prph2*$^{C/+}$ and *Prph2*$^{C/+}$/*Rom1*$^{+/-}$ (Fig. 3A, C, E). Similarly, there was no difference in photopic ERG amplitude between *Prph2*$^{C/+}$ and *Prph2*$^{C/+}$/*Rom1*$^{+/-}$ (Fig. 3B, D, F) at either timepoint examined. These results suggest that overall, reducing *Rom1* has very little to no effect on the *Prph2*$^{C/+}$ model. As a result, this model was not included in subsequent studies.

To determine whether the functional studies had structural correlates, we next examined retinal structure via light microscopy and assessed photoreceptor degeneration by counting nuclei in the outer nuclear layer (largely a reflection of rods since they comprise ~95% of the murine photoreceptors). Retinal lamination was normal in all models (Fig. 4A), and no significant degeneration was observed in the *Rom1*$^{+/-}$ at either P30 or P90. At P30, we observed only minor retinal degeneration

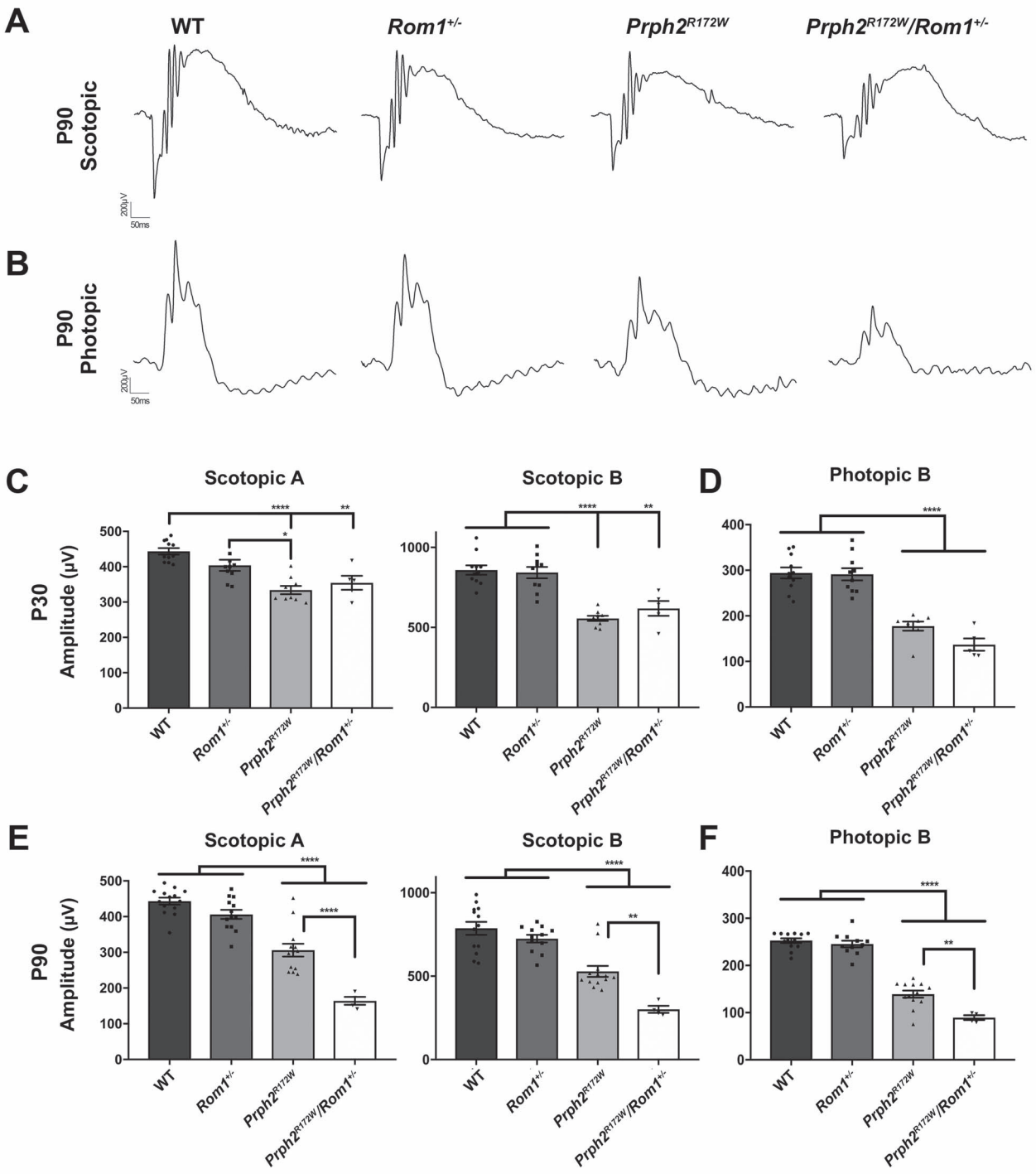

Figure 2. Partial ablation of *Rom1* accelerates rod and cone functional decline in the *Prph2*^{R172W}. Full-field ERG was performed at P30 and P90. (**A**-**B**) Representative waveforms are shown from full-field ERGs collected at P90 under both scotopic (A) and photopic (B) conditions. (**C**-**E**) Plotted are mean ± SEM scotopic a- and b-wave at P30 (C) and P90 (E), and mean ± SEM photopic b-wave at P30 (D) and P90 (**F**). $^{*}P < 0.05$, $^{**}P < 0.01$, $^{***}P < 0.001$ by one-way ANOVA with Tukey's *post-hoc* comparison. $N = 4$–15 animals/genotype. For comparison sake, control values are re-plotted from Figure 1.

in the *Prph2*$^{K/+}$ and *Prph2*$^{K/+}$/*Rom1*$^{+/-}$ versus WT (Fig. 4A and B, top). This degeneration was progressive, by P90, both the *Prph2*$^{K/+}$ and *Prph2*$^{K/+}$/*Rom1*$^{+/-}$ exhibited significant photoreceptor degeneration compared with WT and *Rom1*$^{+/-}$ (Fig. 4A and B, bottom). However, the *Prph2*$^{K/+}$ and *Prph2*$^{K/+}$/*Rom1*$^{+/-}$ were not significantly different from each other at either timepoint, suggesting that early scotopic functional improvements in the *Prph2*$^{K/+}$/*Rom1*$^{+/-}$ versus *Prph2*$^{K/+}$ were not due to slowed retinal degeneration.

No significant retinal degeneration was also observed in the *Prph2*^{R172W} at either P30 or P90, consistent with our finding that rods are well preserved (compared with cones) in this model

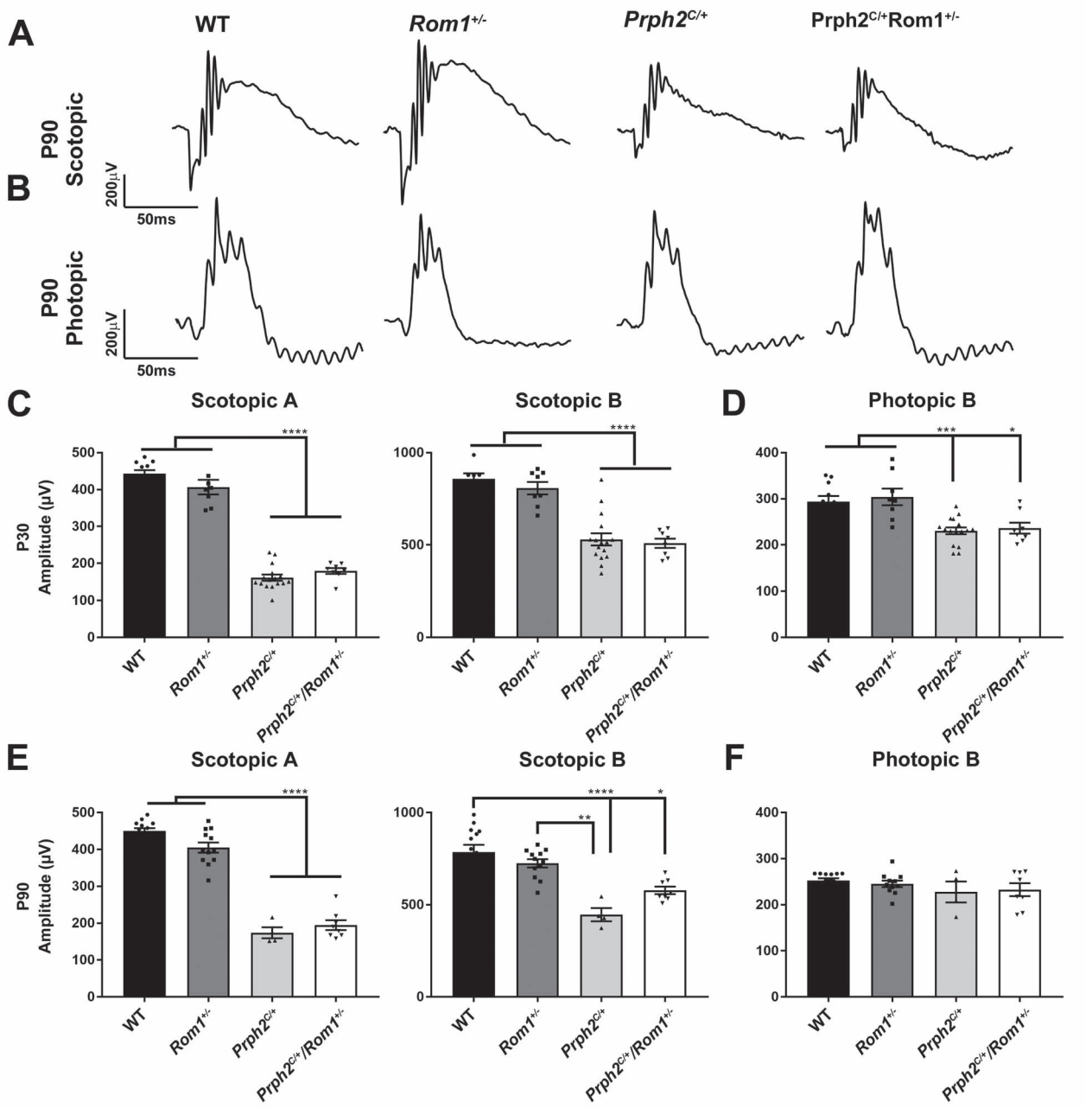

Figure 3. Partial ablation of *Rom1* has little effect on retinal function in the *Prph2*$^{C/+}$. Full-field ERG was performed at P30 and P90. (**A**-**B**) Representative waveforms are shown from full-field ERGs collected at P30 under both scotopic (A) and photopic (B) conditions. (**C**-**E**) Plotted are mean ± SEM scotopic a- and b-wave at P30 (C) and P90 (E), and mean ± SEM photopic b-wave at P30 (D) and P90 (**F**). *$P < 0.05$, ***$P < 0.001$, ****$P < 0.0001$ by one-way ANOVA with Tukey's *post-hoc* comparison. N = 4–15 animals/genotype. For comparison sake, control values are re-plotted from Figure 1.

(17,27,35) (Fig. 4A and C). However, in contrast to the case of the K153Del, removing one allele of *Rom1* in the *Prph2*^{R172W} significantly exacerbated retinal degeneration compared with *Prph2*^{R172W} and WT at both P30 and P90 (Fig. 4A and C). This dramatic acceleration of retinal degeneration in the *Prph2*^{R172W}/*Rom1*$^{+/-}$ was consistent with both our ERG findings and observations from R172W patients with ROM1 variants (20).

PRPH2 trafficking is unaffected by knockdown of *Rom1*

Previously, we found that removing *Rom1* led to mistrafficking of mutant Y141C PRPH2 but not WT PRPH2, suggesting that ROM1 might help guide or promote OS targeting of mutant forms of PRPH2 (22). To help evaluate whether this occurred with other *Prph2* mutations, we performed immunofluorescence on retinal sections from our models with reduced ROM1. Sections from P30 (Supplementary Material, Fig. S1) and P90 were labeled with antibodies that recognize both WT and mutant PRPH2 (green, Fig. 5A) and ROM1 (red, Fig. 5A). As expected, PRPH2 and ROM1 localize to the OS in both WT and *Rom1*$^{+/-}$ retinas, and no mistrafficking of PRPH2 is seen in either the *Prph2*$^{K/+}$ or the *Prph2*$^{K/+}$/*Rom1*$^{+/-}$. A small amount of PRPH2 is detected in the inner segments in the *Prph2*^{R172W} (arrows, Fig. 5A); however, the pattern of this labeling is not different between the *Prph2*^{R172W}

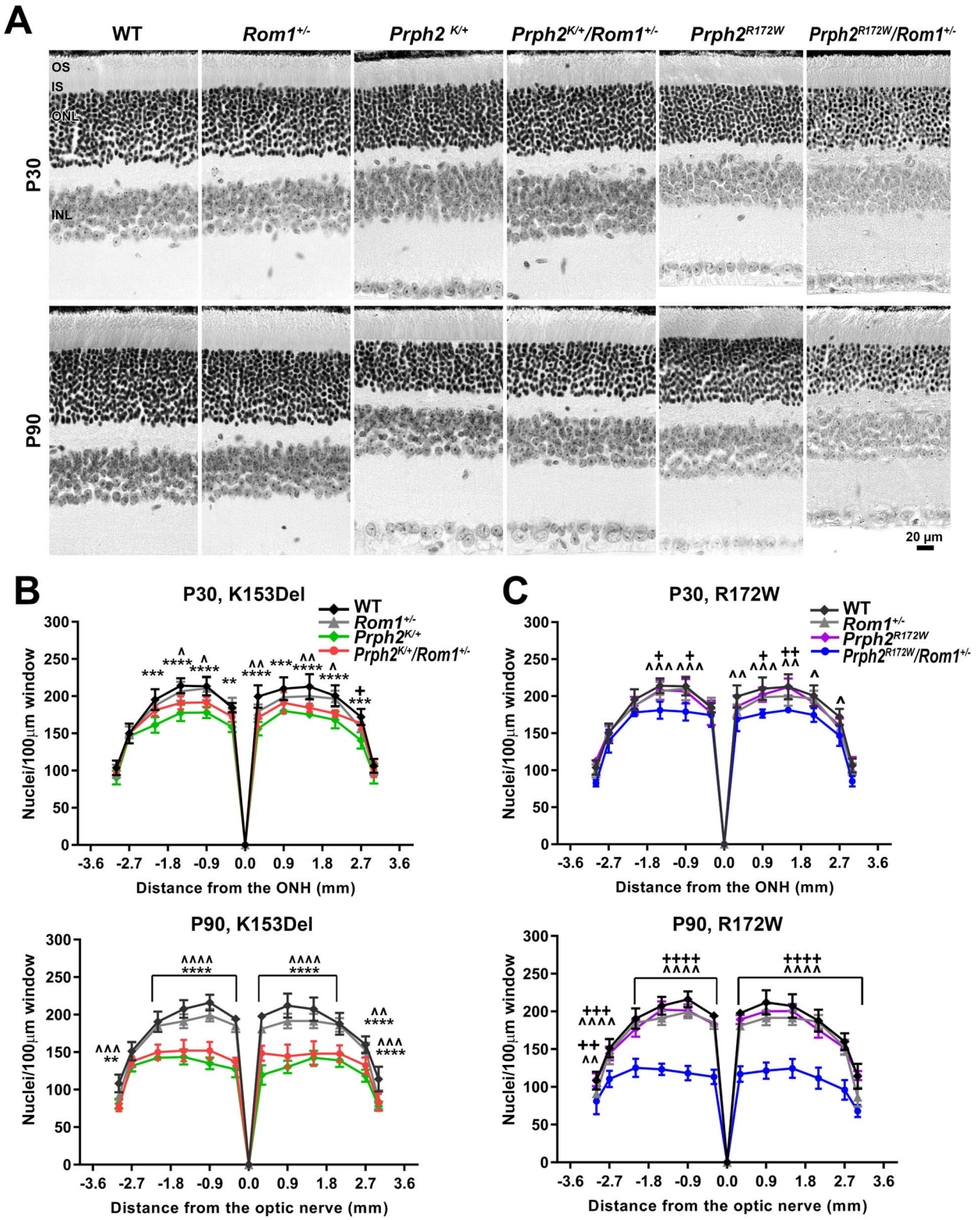

Figure 4. Partial ablation of *Rom1* accelerates ONL thinning in the *Prph2*^{R172W}. (**A**) Representative light microscopic images of H&E stained retinal sections are shown from the indicated genotypes at P30 (top) and P90 (bottom). (**B-C**) Sections were imaged at 500 µm intervals and ONL nuclei within a 100 µm window were counted in animals on the K153Del background (B) or R172W background (C). For comparisons sake, controls are plotted in both (B-C). Plotted are means ± SD. Scale bar: 20 µm. $N = 3$–4 eyes/genotype. OS: outer segment, IS: inner segment, ONL: outer nuclear layer, INL: inner nuclear layer. Differences between genotypes were analyzed by two-way ANOVA with Tukey's *post-hoc* tests. One symbol: $P < 0.05$, two symbols $P < 0.01$, three symbols $P < 0.001$ and four symbols $P < 0.0001$. * denote comparisons between WT versus *Prph2*$^{K/+}$. ^ denote comparisons between WT versus *Prph2*$^{K/+}$/*Rom1*$^{+/-}$ or WT versus *Prph2*^{R172W}/*Rom1*$^{+/-}$. + denote comparisons between *Prph2*$^{K/+}$ and *Prph2*$^{K/+}$/*Rom1*$^{+/-}$ or *Prph2*^{R172W} versus *Prph2*^{R172W}/*Rom1*$^{+/-}$.

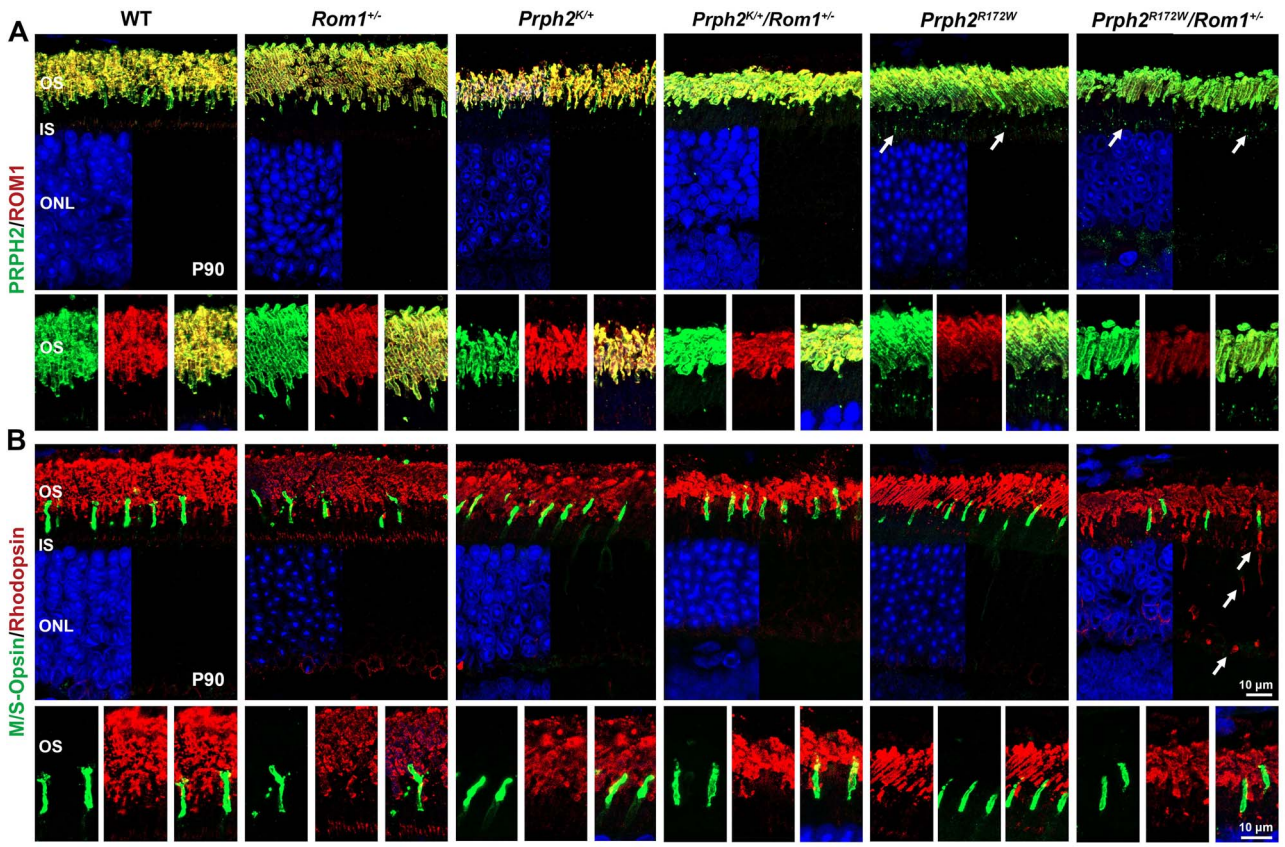

Figure 5. Partial ablation of *Rom1* does not impair OS trafficking of PRPH2 or ROM1. (**A-B**) Retinal sections of the indicated genotypes collected at P90 were labeled with antibodies against PRPH2 (green) and ROM1 (red) (A), or rhodopsin (red) and a mix of antibodies against M- and S-opsin (green) (B). Smaller panels below show expanded views of individual channels. Arrowheads highlight abnormal accumulation of proteins in the IS or outer nuclear layer. Scale bars: 10 µm. OS: outer segments, IS: inner segments, ONL: outer nuclear layer.

and *Prph2*^{R172W}/*Rom1*$^{+/-}$. These findings suggest that reducing ROM1 levels does not affect OS targeting of R172W or K153Del PRPH2.

Mislocalization of rhodopsin and cone opsins (M/S-opsins) also often accompanies retinal degeneration and/or photoreceptor OS dysmorphism. To determine whether opsins were mislocalized in our models, we labeled retinal sections for rhodopsin and M/S-opsins (using a mix of antibodies against M/S-opsin). We did not see any mislocalization of M/S-opsins at either P30 (Supplementary Material, Fig. S1) or P90 (Fig. 5B) in any models. Rhodopsin was properly localized to the OS in the WT, *Rom1*$^{+/-}$, *Prph2*$^{K/+}$ and *Prph2*$^{K/+}$/*Rom1*$^{+/-}$ with a small amount of newly synthesized rhodopsin often visible in a line at the base of the IS. Rhodopsin was also properly localized in the *Prph2*^{R172W}; however, substantial rhodopsin mislocalization in the inner segment and outer nuclear layer was observed in the *Prph2*^{R172W}/*Rom1*$^{+/-}$ (arrows, Fig. 5B), consistent with the data indicating that rod function and degeneration are worse in this model than in the *Prph2*^{R172W}.

PRPH2/ROM1 complex formation is altered when ROM1 is reduced

Normally PRPH2 and ROM1 oligomerize into a variety of complexes, including homo- and hetero-tetramers, homo- and hetero-octamers, and larger PRPH2 homo-oligomers, which are held together through both non-covalent bonds and disulfide linkages. However, one frequent biochemical outcome of *Prph2* mutations is alteration in the formation of these protein complexes. For example, mice carrying the Y141C mutation accumulate abnormal high molecular weight complexes which are larger than normal PRPH2 oligomers (22). These complexes also contain ROM1, which is not usually found in the largest PRPH2 complexes. When we removed ROM1 from Y141C *Prph2* mice, however, these abnormal PRPH2/ROM1 complexes were eliminated (23). To determine whether these biochemical findings on the role of ROM1 were applicable across multiple mutations, we here evaluated complex assembly in *Prph2*$^{K/+}$ with varying levels of ROM1. The R172W mutation does not cause significant alterations in complex formation, so those retinas were not included in this experiment (27,28,35).

We performed SDS–PAGE/western blots using P30 retinal extracts. Under non-reducing conditions, disulfide-linked PRPH2/ROM1 complexes appear as dimers, whereas non-covalently linked complexes run as monomers. In WT, *Rom1*$^{+/-}$, and *Rom1*$^{-/-}$, PRPH2 and ROM1 are only present in the expected dimer and monomer bands (Fig. 6A). We also observed the previously described abnormal large molecular weight PRPH2/ROM1 complexes in *Prph2*$^{K/+}$ retinas (Fig. 6A, arrows). However, removal of either one or both alleles of *Rom1* leads to a dose-dependent decrease in the formation of these abnormal high molecular weight PRPH2/ROM1 complexes (arrows, Fig. 6A). Even in *Prph2*$^{K/+}$*Rom1*$^{-/-}$ retinas, a small amount of the abnormal high molecular weight PRPH2 complex remains, suggesting that the formation of these complexes is not entirely dependent on ROM1. These abnormal high molecular weight

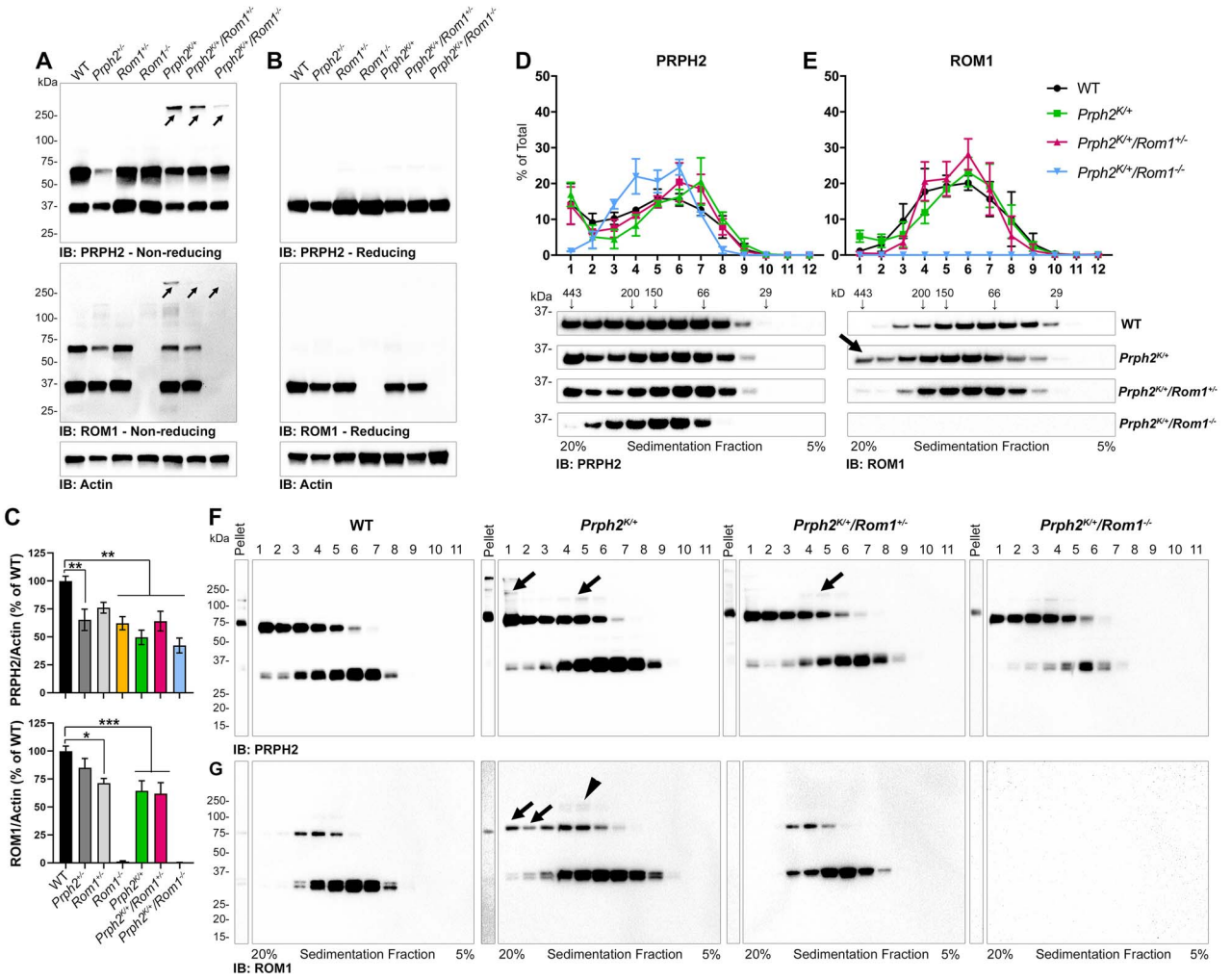

Figure 6. Elimination of *Rom1* improves defects in PRPH2/ROM1 complex formation in the $Prph2^{K/+}$. (**A**-**B**) P30 retinal extracts from the indicated genotypes were separated by SDS–PAGE/western blot under both (A) non-reducing and (B) reducing conditions. Arrows indicate the abnormal large MW complexes. (**C**) Plotted is mean ± SEM levels of PRPH2 and ROM1 protein at P30 from the indicated genotypes. $N = 9$ retinas/genotype. $^{*}P < 0.05$, $^{**}P < 0.01$ and $^{***}P < 0.001$ in one-way ANOVA with Tukey's *post-hoc* comparisons. (**D**-**G**) P30 retinal extracts were separated on continuous 5–20% non-reducing sucrose gradients. Gradient fractions were collected and analyzed using both (D-E) reducing and (F-G) non-reducing SDS-PAGE/western blots. (D-E) Reducing SDS–PAGE/western blots were probed with PRPH2 (D) and ROM1 (E) antibodies, and the percent of total PRPH2 or ROM1 in each gradient fraction was plotted (mean ± SEM). (F-G) Non-reducing SDS–PAGE/western blots are shown from gradient fractions. (F) Arrows indicate accumulation of large PRPH2 complexes with abnormal disulfide linkages in fractions 1–5. (G) Arrows highlight abnormal inclusion of ROM1 into fractions 1–3. Arrowheads highlight ROM1 with additional disulfide linkages.

complexes are efficiently eliminated under reducing conditions (Fig. 6B), suggesting they are not non-specific protein aggregates. Quantification of reducing western blots demonstrated that PRPH2 levels were significantly reduced in the $Prph2^{K/+}$ (Fig. 6C). Levels in the $Prph2^{K/+}/Rom1^{+/-}$ were slightly higher than in the $Prph2^{K/+}$, although the improvement was not statistically significant and levels in the $Prph2^{K/+}/Rom1^{+/-}$ were still significantly lower than WT. PRPH2 levels in the $Prph2^{K/+}/Rom1^{-/-}$ were similar to those in the $Prph2^{K/+}/Rom1^{+/-}$. These data suggest that the stability of K153Del PRPH2 is not significantly affected by removing ROM1. ROM1 levels were similarly reduced in the $Rom1^{+/-}$, $Prph2^{K/+}$ and $Prph2^{K/+}/Rom1^{+/-}$ compared with WT (Fig. 6C).

Non-reducing western blots help to determine the distribution of covalent versus non-covalently linked PRPH2/ROM1 complexes, but to further evaluate PRPH2/ROM1 oligomerization, we performed sucrose gradient sedimentation using continuous 5–20% gradients (under non-reducing conditions). PRPH2/ROM1 homo- and hetero-tetramers are found in sedimentation fractions 6–9. Subsequently, these core complexes further assemble into PRPH2/ROM1 homo and hetero-octamers (fractions 4–5) and higher order PRPH2 homo-oligomers (fractions 1–3). To evaluate overall complex distribution, gradient fractions are separated via reducing SDS–PAGE/western blot and the percent of total PRPH2 or ROM1 in each gradient fraction is plotted (Fig. 6D and E). The overall distribution of PRPH2 complexes does not undergo a significant shift in the $Prph2^{K/+}$ or $Prph2^{K/+}/Rom1^{+/-}$ retina. In the $Prph2^{K/+}/Rom1^{-/-}$ retina, we observe that there is a slight right-shift in PRPH2 distribution toward intermediate sized complexes (Fig. 6D, blue line). We have previously observed this pattern in the $Rom1^{-/-}$ (13), suggesting that in the absence of ROM1, additional PRPH2 accumulates in intermediate sized complexes (fractions 4–5) at the expense of higher order complexes (likely to compensate for the loss of ROM1). ROM1 is

normally excluded from the heaviest fractions (1–3). However, in the *Prph2*$^{K/+}$, we observed ROM1 in these fractions, suggesting that ROM1 is recruited into large PRPH2 complexes that are normally homomeric (Fig. 6E, green line and arrow). This abnormal accumulation of ROM1 in fractions 1–3 is largely ameliorated in the *Prph2*$^{K/+}$/*Rom1*$^{+/-}$.

Evaluation of gradient fractions under non-reducing conditions (Fig. 6F and G) provided further insight into PRPH2/ROM1 complex abnormalities. *Prph2*$^{K/+}$ retinas exhibit accumulation of large PRPH2 complexes with abnormal disulfide linkages in fractions 1–5 (Fig. 6F, second panel, arrows). Critically, these abnormal PRPH2 complexes are largely removed when ROM1 levels are reduced or eliminated (Fig. 6F, third and fourth panels, arrows), consistent with findings from non-reducing western blots (Fig. 6A). Probing non-reducing gradient blots for ROM1 shows that the abnormal ROM1 that we observed in higher order complexes in the *Prph2*$^{K/+}$ (refer back to Fig. 6E) is largely disulfide linked (Fig. 6G, arrows, second panel). Some ROM1 with additional disulfide linkages is also observed in the *Prph2*$^{K/+}$ (Fig. 6G, arrowhead, second panel). However, abnormal ROM1 complexes are not present in the *Prph2*$^{K/+}$/*Rom1*$^{+/-}$ (Fig. 6G, third panel). Combined, these findings suggest that reducing ROM1 ameliorates defects in PRPH2/ROM1 complex assembly associated with the K153Del mutation in *Prph2*.

OSs depend on having sufficient PRPH2 and proper PRPH2 complexes to form correctly sized and shaped disks. To determine whether OS ultrastructure was affected by removing one allele of *Rom1*, we performed EM on retinal sections at P90 (Fig. 7). WT and *Rom1*$^{+/-}$ OSs were well-structured with nicely stacked disks. In the *Prph2*$^{K/+}$, OSs were shorter and disorganized (Fig. 7A). Gross OS structure was not improved in the *Prph2*$^{K/+}$*Rom1*$^{+/-}$, a finding supported by our observation that rhodopsin levels (a biochemical proxy for overall amount of OS) are similarly reduced in the *Prph2*$^{K/+}$ and *Prph2*$^{K/+}$/*Rom1*$^{+/-}$ (Fig. 7C). However, examination at higher magnification (Fig. 7B) showed that removing one allele of *Rom1* did lead to slight ultrastructural improvements. In the *Prph2*$^{K/+}$, OSs were frequently filled with accumulated membranous debris and unflattened disks/vesicles that impaired disk stacking (arrowheads, Fig. 7B). However, in the *Prph2*$^{K/+}$*Rom1*$^{+/-}$, this debris in the OS was not as evident. Most OSs, though short and with abnormally sized disks, exhibited disks that stacked nicely (Fig. 7B, arrows). Although tissues for EM were not available for the *Prph2*$^{K/+}$/*Rom1*$^{-/-}$, rhodopsin levels were as low as those in the *Prph2*$^{K/+}$, suggesting that full removal of *Rom1* is unlikely to lead to drastically improved ultrastructure (Fig. 7C).

Discussion

Our goal in this project was to understand the extent to which the effects of reducing or removing *Rom1* were applicable across multiple *Prph2* mutations and to determine whether these effects required complete removal or just reduction in *Rom1*. Both of these questions have direct clinical and translational implications. *PRPH2*-associated disease has widely varying disease presentation and multiple complicated molecular mechanisms, so the search for commonalities or identification of factors to help explain this variability is essential. In addition, patients are genetically more likely to have a single null *ROM1* variant than two, so understanding whether partial ablation of *ROM1* has an effect at the molecular/cellular level is an important part of the overall picture of *ROM1* as a modifier of *PRPH2*-associated disease. Here we clearly show, on the structural, functional and molecular level, that removing a single allele of *Rom1* affects *Prph2*-associated disease phenotypes, supporting findings from human studies in *PRPH2* patients with *ROM1* variants (20). However, critically, we also observe that the effects of removing one allele of *Rom1* are not similar across *Prph2* mutations. In the case of the K153Del mutation, removal of one allele of *Rom1* results in modest functional improvements in rods and cones. In contrast, in the case of the R172W mutation, removing an allele of *Rom1* is highly deleterious to both rods and cones, while there is no effect in mice with the C213Y mutation. Combined with our previous findings in the Y141C model (23), it is clear that while reducing *Rom1* can modify phenotypes associated with several different *Prph2* mutations, these effects are not consistent across mutations.

Insight into potential mechanisms underlying these differences in the effects of *Rom1* can be gained by closer examination of the individual mutations. All four of the mutations we examined here (and previously) reside in the PRPH2 D2 loop (Fig. 8), the region known to be essential for PRPH2 oligomerization. Several important characteristics of this region have been mapped, including a region required for PRPH2/PRPH2 interactions, a larger region required for PRPH2/ROM1 interactions (36), cysteines involved in intramolecular disulfide bonds (critical for D2 loop folding) (10) and cysteines involved in intermolecular disulfide bonds (critical for disulfide-linked oligomerization) (10,37,38). The effects of reducing *Rom1* on the C213Y mutation are the most straightforward to understand. This mutation impairs formation of an intramolecular disulfide linkage severely affecting overall D2 loop folding and PRPH2 stability. As a result, even though C213 does not reside in the region required for PRPH2/ROM1 assembly, C213Y PRPH2 cannot interact with ROM1 (26). Therefore, our finding here that removing an allele of *Rom1* has little effect on C213Y-associated phenotypes is consistent with our understanding of the molecular basis of C213Y-associated disease.

The other three mutants all reside within areas known to be important for PRPH2/PRPH2 or PRPH2/ROM1 assembly (Fig. 8); however, none of these three mutants have effects on PRPH2 oligomerization as severe as C213Y. We find that eliminating one allele of *Rom1* has severe effects on photoreceptor structure and function in the *Prph2*^{R172W}, yet, the R172W mutation has very few effects on complex formation at all; and subtle defects in oligomerization are only observed in cones on the *Nrl*$^{-/-}$ background (27). This is similar to the case of the L185P mutant, which is near R172W and is associated with digenic retinitis pigmentosa (16,18). Like R172W, L185P PRPH2 forms complexes with WT PRPH2 (39), and in patients, predicted *ROM1* null alleles either contribute to or worsen disease outcomes (16,18,20). However, analysis of the L185P mutation in mouse models with reduced *Rom1* did not provide further insight into how *ROM1* mutations contribute to disease (19). In addition, L185P and R172W are not completely analogous; patients with only L185P (i.e. without *ROM1* mutations) are asymptomatic (18), while R172W causes clear macular dystrophy (16,18,33,34). We do know that cones are sensitive to the ratio of PRPH2/ROM1, and that overexpression of ROM1 is toxic to cones (40). It is thus formally possible that exacerbation of phenotypes in *Prph2*^{R172W}/*Rom1*$^{+/-}$ retinas is tied to changes in the PRPH2/ROM1 ratio. However, in *Prph2*^{R172W}/*Rom1*$^{+/-}$ retinas, the PRPH2/ROM1 ratio is increased, not decreased, and increasing the PRPH2/ROM1 ratio by removing ROM1 does not severely affect either cone or rod function (13,15), so this is unlikely to account for exacerbation of degeneration in the *Prph2*^{R172W}/*Rom1*$^{+/-}$. Given the severe functional and structural effects of reducing *Rom1* in the *Prph2*^{R172W}, coupled

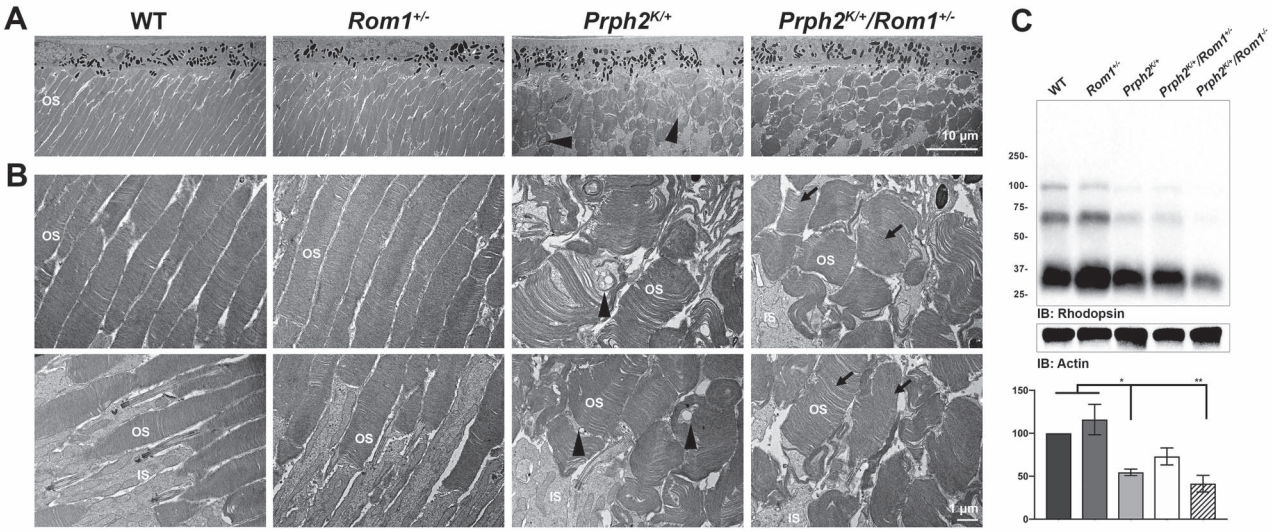

Figure 7. Partial ablation of *Rom1* improves OS ultrastructure in the *Prph2*$^{K/+}$. (**A-B**) Representative transmission EM are shown from the indicated genotypes at P90. Arrowheads highlight abnormal membranous/vesicular inclusion in the OS of *Prph2*$^{K/+}$ retinas. Arrows highlight improved disk stacking in the *Prph2*$^{K/+}$/*Rom1*$^{+/-}$. Images in (A) were captured at 500x magnification, while higher magnification images in (B) were captured at 2500x (C). Rhodopsin protein levels were assessed by SDS–PAGE/western blot and quantified. Plotted are means ± SEM. N = 5 retinas/genotype. Scale bars: 10 µm (A) and 1 µm (B).

with observations supporting the clinical relevance of this finding (20), investigations to further elucidate underlying molecular mechanisms for worsened phenotypes in R172W animals with reduced *Rom1* are warranted.

In contrast to R172W, the Y141C and K153Del mutations both cause the formation of abnormally large molecular weight, disulfide linked complexes (22,25), and in both cases, the formation of these complexes is reduced or eliminated by removing *Rom1* (23). In addition, removing *Rom1* in the Y141C retina improved cone function at an early timepoints (P30), and reducing *Rom1* in the K153Del retina slowed cone degeneration at P90. These findings suggest that correcting abnormalities in PRPH2/ROM1 complex formation by reducing *Rom1* can be beneficial for cones. This is consistent with the overall paradigm that cones are more sensitive to having correctly formed PRPH2 complexes, whereas rods are more sensitive to the total quantity of PRPH2 present (4,27,41–43). Interestingly the effects of reducing *Rom1* on rod function differ in the Y141C versus K153Del mutants. Scotopic ERG responses were much worse in *Prph2*$^{Y141C/+}$/*Rom1*$^{-/-}$ versus *Prph2*$^{Y141C/+}$ animals, while *Prph2*$^{K/+}$/*Rom1*$^{+/-}$ had improved scotopic ERGs compared with *Prph2*$^{K/+}$. In the Y141C, we attributed reduced scotopic ERGs after removal of *Rom1* to the fact that elimination of ROM1 led to decreased stability of Y141C mutant protein and thus dramatic reductions in total PRPH2 (23). Rods are extremely sensitive to PRPH2 haploinsufficiency, so it makes sense that reduced PRPH2 levels would lead to reductions in rod function. However, this reduced PRPH2 stability after removal of ROM1 does not occur with the K153Del mutant. Prph2 levels are slightly higher in the *Prph2*$^{K/+}$/*Rom1*$^{+/-}$ compared with *Prph2*$^{K/+}$ and not different in the *Prph2*$^{K/+}$ versus the *Prph2*$^{K/+}$/*Rom1*$^{-/-}$. This difference in PRPH2 stability in the absence of ROM1 in the K153Del versus Y141C provides a logical explanation for differing scotopic ERG responses in Y141C versus K153Del retinas with reduced ROM1, but it remains unclear why ROM1 should promote the stability of Y141C but not K153Del PRPH2.

Previously, we observed that PRPH2 trafficking was severely impaired in the Y141C model in the absence of ROM1, suggesting that ROM1 might promote trafficking of mutant forms of PRPH2 (23). PRPH2 traffics through both an unconventional secretory pathway which bypasses the trans-Golgi (44) and conventional trafficking pathways, and support for a role for ROM1 in trafficking comes from our findings that ROM1 promotes conventional trafficking of PRPH2 (13,45). Here, we did not observe any differences in PRPH2 trafficking in either the K153Del or the R172W when one allele of *Rom1* was removed. This may be because these mutants do not misfold sufficiently to require assistance from ROM1. However, it is important to note that in the clinically relevant models used here, we studied mice heterozygous for both *Prph2* mutation and *Rom1* knockout, so both WT PRPH2 and ROM1 are still present, making comparisons with our findings from the *Prph2*$^{Y141C/Y141C}$/*Rom1*$^{-/-}$ difficult. Our findings here do indicate that in patients with autosomal dominant *PRPH2*-associated disease, effects of *ROM1* variants (deleterious or beneficial) are unlikely to be tied to PRPH2/ROM1 trafficking to the OS.

Finally, what do these findings suggest about potential therapies for PRPH2-associated retinal dystrophies? Many attempts at gene supplementation for *Prph2*-associated disease have been tried. Genetic supplementation in mouse models (i.e. overexpression of WT PRPH2 via transgenesis) has been effective in cases of haploinsufficiency or in loss-of-function mutations like C214S (46,47). However, this approach has been less successful in the case of mutations with gain-of-function/dominant-negative effects including R172W, K153Del and C213Y (25,26,35). Gene supplementation via gene therapy has also been tried (48–50), but is even more difficult given the need for the retina to have high levels of PRPH2 to function properly. This approach also ignores the effects of dominant negative/gain-of-function mutations, which would need to be knocked down to overcome deleterious effects. A simultaneous knockdown/gene replacement strategy is likely needed (51,52), and development of effective approaches in this area has been challenging. Given the role of *ROM1* as a modifier gene for *PRPH2*-associated disease, either supplementation or knockdown of *ROM1* might be a therapeutic approach to improve *PRPH2*-associated disease. However, our findings show that the effects of removing or reducing *Rom1* are variable and

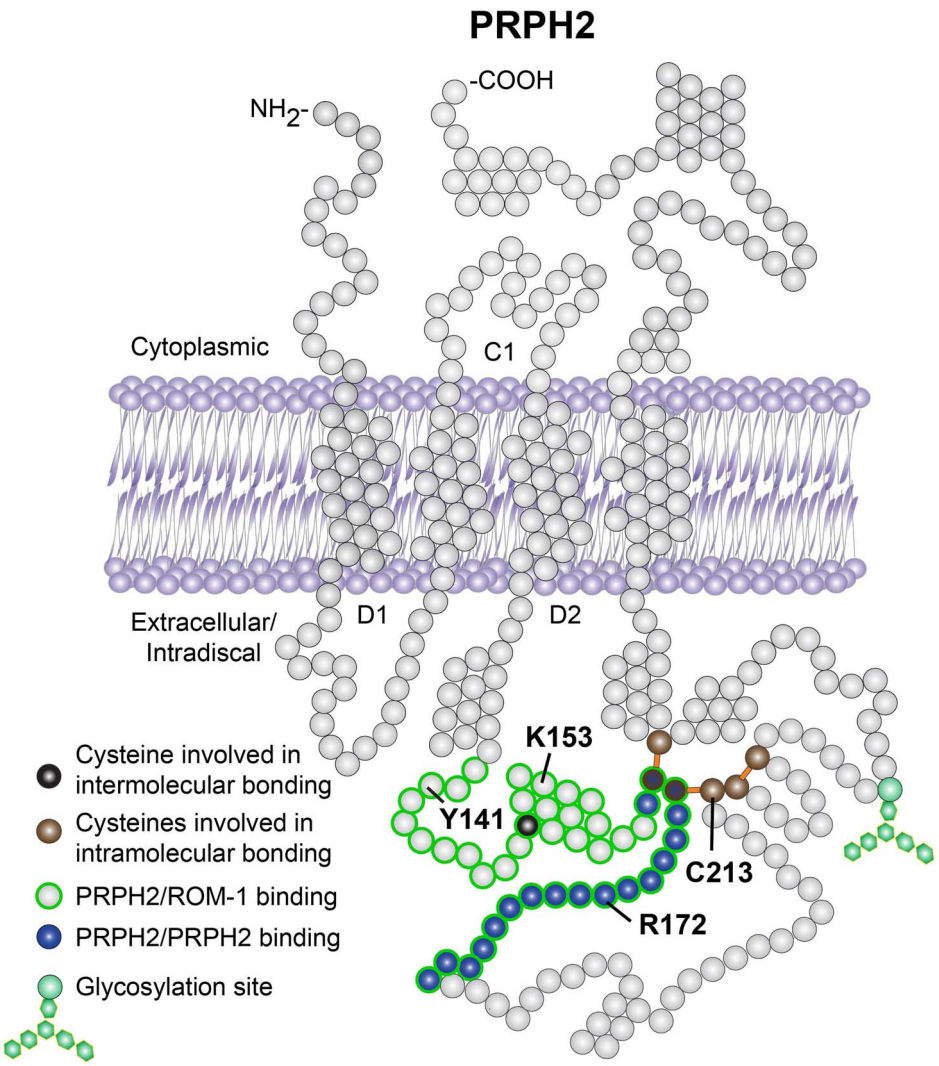

Figure 8. Diagram of the PRPH2 molecule highlighting relevant disease mutants. Shown is a diagram of the mouse PRPH2 protein, with relevant functional domains and disease mutants indicated. Modified from (26).

also unpredictable (given the large number of uncharacterized *PRPH2* disease mutations). Even in cases where reducing *Rom1* is beneficial (e.g. K153Del), the benefits are only partial and in other cases, reducing *Rom1* is deleterious. While this might suggest that *Rom1* supplementation would be beneficial, our previous studies have shown that overexpression of *Rom1* can be toxic (40), and findings both here and elsewhere suggest that the PRPH2/ROM1 ratio is important for retinal health. While our results provide substantial insight into PRPH2-associated phenotypic heterogeneity, it seems unlikely that *Rom1* is a viable therapeutic target in patients with *PRPH2*-associated disease.

In conclusion, we here present strong evidence that reducing *Rom1* can modify disease phenotypes in multiple clinically relevant *Prph2* mutants. This leads to the question of whether or to what extent *ROM1* null variants occur in the human population. Because *ROM1* is not a primary retinal disease gene like *PRPH2* or rhodopsin, it has received much less research focus. However, the advent of next generation sequencing methods means that extensive genetic information is now more readily available, and hundreds of *ROM1* gene variants have been reported, for example in public genomics databases such as gnomAD (https://gnomad.broadinstitute.org/) (53). Though some of these are frameshift or other variants likely to be loss-of-function alleles, many more are missense variants (which may or may not be loss-of-function) or variants of unknown significance. Future comprehensive human genetics studies will be needed to help determine to what extent *ROM1* null variants exist in the wider population and to what extent they may contribute to phenotype in *PRPH2*-disease patients. Importantly, the effects of a *Rom1* null allele are not the same across different *Prph2* mutants, underscoring the complex nature of *PRPH2*-asscoiated diseases. These studies provide substantial cellular and molecular evidence that *ROM1* acts as a *PRPH2* disease modifier, and further investigation into the presence of *ROM1* variants in patients may help in our understanding of *PRPH2*-associated phenotypic heterogeneity and contribute to more accurate prognosis in patients.

Materials and Methods

Animal care and use

Animal maintenance and experiments were approved by the local Institutional Animal Care and Use Committee (IACUC; University of Houston, TX) and adhered to guidelines from

the Association for Research in Vision and Ophthalmology (Rockville, MD). The previously characterized K153 and C213Y *Prph2* lines have point mutations knocked into the endogenous *Prph2* locus and are here used as heterozygotes (one mutant and one WT allele), abbreviated $Prph2^{K/+}$ and $Prph2^{C/+}$, respectively (25,26). The previously characterized R172W *Prph2* line is transgenic, in which expression of R172W mutant *Prph2* is driven in photoreceptors by the hIRBP promoter (human interphotoreceptor retinoid binding protein) (27,28,35). Mice used here are hemizygous for R172W and homozygous for WT *Prph2* (abbreviated $Prph2^{R172W}$), and we have previously shown that one allele of the R172W transgene generates PRPH2 protein levels ~40% of WT PRPH2 levels (28). To control for potential effects of overexpression, we previously demonstrated that overexpressing WT PRPH2 at levels comparable with those in R172W hemizygotes did not have any deleterious effects in the retina (46). $Rom1^{-/-}$ knockout mice have also been previously characterized, and $Rom1^{-/-}$ mice used here were bred from founders originally provided by Dr Roderick McInnes (McGill University, Montreal, Canada) (15,23). Animals were raised under cyclic lighting conditions (12 h L/D, ~30 lux). All mice were backcrossed onto our in-house WT strain. This strain was created by breeding FVB mice to C57BL/6, eliminating the *rd1* and *rd8* mutations and then inbreeding for over 10 generations. $Rom1^{-/-}$ animals breed poorly, and in most cases mice homozygous for the *Rom1* knockout allele ($Rom1^{-/-}$) and heterozygous for *Prph2* mutations were unobtainable. Frequently, mice that were born exhibited unhealthy phenotypes (microcephaly, small size, failure to thrive, etc.). These systemic phenotypes are also often seen in $Rom1^{-/-}$ suggesting they do not relate to addition of *Prph2* mutations but rather to the $Rom1^{-/-}$ line. $Rom1^{+/-}$ animals did not exhibit any systemic defects compared with WT littermates. Animal groups were not randomized, but all groups included both male and female mice. No animals were excluded from the study unless they were euthanized for meeting a humane endpoint as described in the IACUC protocol, or if eyes were grossly injured/abnormal. These criteria are used in all our studies.

Electroretinography

Full-field ERGs were performed as previously described (23,25). After overnight dark adaptation, animals were anesthetized by intramuscular injection of 85 mg/kg ketamine and 14 mg/kg xylazine (Butler Schein Animal Health, Dublin, OH). Eyes were subsequently dilated with 1% cyclopentolate solution (Akorn, Inc., Lake Forest, IL). ERGs were performed with a UTAS system (LKC, Gaithersburg, MD). Rod photoreceptor function (scotopic ERG) was recorded with a strobe flash stimulus of 157 cd-s/m^2 presented to the dark-adapted mouse. Mice were then subjected to background light adaptation for 5 min at 29.03 cd/m^2. Cone photoreceptor function (photopic ERG) was recorded from 25 averaged flashes at 157 cd-s/m^2 with white light.

Histology

Eyes were enucleated and fixed overnight in Davidson's fixative (32% ethanol, 11% acetic acid, 2% formaldehyde) at 4°C. Subsequently, the eyes were dehydrated, embedded in paraffin and sectioned at 10 µm thickness. Sections were stained with hematoxylin and eosin (H&E) according to standard protocols, and images were captured using a Zeiss Axioskop equipped with a Zeiss Axiocam (Zeiss, Jena, Germany) and a 20x objective lens. For morphometry, images were captured every 0.5 mm, beginning at the optic nerve and moving peripherally (superiorly and inferiorly). Images were analyzed using ImageJ software. Nuclei were counted in 100 µm wide portions of retina, centered at the indicated distance from the optic nerve. Nuclei were counted in the ONL only, and counts were recorded manually using ImageJ software.

Transmission electron microscopy

Eyes were collected, processed, and plastic-embedded for transmission electron microscopy (EM) as described previously (54). Thin sections (600–800 Å) collected on copper 75/300 mesh grids were then stained with 2% uranyl acetate and Reynolds' lead citrate for transmission EM. EM images were collected using a JEOL 100CX EM at an accelerating voltage of 60 kV.

Antibodies

Primary antibodies used for all immunoblotting and immunofluorescence staining are summarized in Table 1.

Immunofluorescence labeling

Eyes were processed and immunostained as previously described for paraffin sections (25). In short, slides were deparaffinized and rehydrated then underwent antigen retrieval in sodium citrate buffer for 30 minutes (10 mM sodium citrate, 0.05% Tween 20, pH 6.0, heated to 100°C). Slides were washed in 1X PBS, blocked for 1 h (5% BSA, 1% donkey serum, and 1X PBS pH 7.0), and incubated with primary antibodies overnight at 4°C. The following day, slides were washed, incubated with secondary antibodies, washed once more, and counterstained with DAPI to visualize nuclei. AlexaFluor conjugated secondary antibodies (Life Technologies/ThermoFisher) were used at 1:1000 dilution. Images were captured using a ZEISS Confocal LSM 900 microscope equipped with a Zeiss Axiocam (Zeiss, Jena, Germany) using a 63× (oil, 1.4 NA) objective and processed using ZEN Image Analysis software (Zeiss, Jena, Germany). Confocal images were taken as an 8 slice stack, at 290 nm per slice, 2.32 µm total and collapsed into a to a single projection image. Figures were then made in Adobe Photoshop.

Immunoblot analysis and velocity sedimentation

Immunoblot and velocity sedimentation were performed as described previously (38,55). Isolated retinas were placed in 100 µl extraction buffer [1X PBS pH 7.0 containing 1% triton-X 100, 5 mM EDTA, 5 mg/ml n-ethylmaleimide (NEM) and a standard protease inhibitor cocktail; chilled to 4°C] per retina, briefly sonicated and incubated at 4°C for 1 h. Protein extracts were then centrifuged for 10 min at 20 000x*g* and 4°C to remove insoluble debris. Protein concentration was quantified via a colorimetric protein assay (Bradford reagent from Bio-rad, Hercules, CA). SDS–PAGE and immunoblotting were performed under both reducing (with β-mercaptoethanol) and non-reducing conditions (without β-mercaptoethanol). Velocity sedimentation was performed using continuous sucrose density gradients of 5–20% with 200 µg protein/sample as described previously (38,55). Twelve gradient fractions and an insoluble pellet fraction were collected from each sample Densitometric quantification was performed on non-saturated blots using Image Lab Software (Bio-Rad, Temecula, CA).

Table 1. Antibodies used. Antibodies used are listed here. WB: western blot, IF: immunofluorescence

Antigen	Species	Clone	Application/Concentration	Source
PRPH2	Rabbit	RDS-CT	1:1000 (WB, IF)	In house (28) RRID:AB_2833006.
ROM-1	Mouse	2H5	1:1000(WB), 1:500 (IF)	In house. Available from Millipore Cat# MABN1757
M-Opsin	Rabbit	Opsin 1 (Medium Wave)	1:1000 (IF)	Novus Biologicals cat# 110–74 730 RRID:AB_1049390
S-Opsin	Rabbit		1:1000 (IF)	Novus Cat# NBP1–20194, RRID:AB_2299094
Rhodopsin	Mouse	1D4	1:2000 (IF)	Gift from R. Molday Can be purchased: Santa Cruz Biotechnology Cat# sc-57 432, RRID:AB_785511
Actin-HRP	Mouse	AC-15	1:50 000 (WB)	Sigma-Aldrich Cat# A3854, RRID:AB_262011
Rabbit IgG HRP	Goat		1:25 000 (WB)	SeraCare KPL Cat# 074–1506, RRID:AB_2721169
Mouse IgG HRP	Goat		1:25 000 (WB)	Millipore Cat# AP130P, RRID:AB_91266
Rabbit IgG Alexa Flour 488	Donkey		1:1000 (IF)	Thermo Fisher Scientific Cat# A-21206, RRID:AB_2535792
Mouse IgG Alexa Fluor 555	Donkey		1:1000 (IF)	Thermo Fisher Scientific Cat# A-31570, RRID:AB_2536180

Statistical analysis

Differences between genotypes were analyzed by one-way ANOVA with Tukey's *post-hoc* comparisons or two-way ANOVA with Tukey's *post-hoc* comparison (when there were two variables). Analysis was done using GraphPad Prism version 8 (GraphPad Software, La Jolla, CA). Significance was set at $P < 0.05$. Throughout the manuscript $^{*}P < 0.05$, $^{**}P < 0.01$, $^{***}P < 0.001$ and $^{****}P < 0.0001$ for indicated pairwise comparisons. For ERG analyses, $N = 1$ represents a single animal. ERG values for both eyes are averaged together to get one value for each animal. For post-mortem analyses, $N = 1$ represents a single retina. However, for any given experiment, all retinas come from different animals, so $N = 5$ retinas/genotype indicates that five individual retinas were analyzed and that they came from five different animals.

Supplementary Material

Supplementary material is available at *HMG* online.

Acknowledgements

The authors thank Mr Alexander Ferrer for his technical assistance and Dr Roderick McInnes for sharing the *Rom1*$^{-/-}$ mouse line.

Conflict of Interest statement. The authors declare they have no conflicts of interest.

Funding

This work was supported by the National Institutes of Health (R01EY10609 to M.I.N. and M.R.A. and NIGMS 1 P20 GM12552801A1 to S.M.C.).

References

1. Arikawa, K., Molday, L.L., Molday, R.S. and Williams, D.S. (1992) Localization of peripherin/rds in the disk membranes of cone and rod photoreceptors: relationship to disk membrane morphogenesis and retinal degeneration. *J. Cell Biol.*, **116**, 659–667.
2. Molday, R.S., Hicks, D. and Molday, L. (1987) Peripherin. A rim-specific membrane protein of rod outer segment discs. *Invest. Ophthalmol. Vis. Sci.*, **28**, 50–61.
3. Jansen, H.G. and Sanyal, S. (1984) Development and degeneration of retina in rds mutant mice: electron microscopy. *J. Comp. Neurol.*, **224**, 71–84.
4. Cheng, T., Peachey, N.S., Li, S., Goto, Y., Cao, Y. and Naash, M.I. (1997) The effect of peripherin/rds haploinsufficiency on rod and cone photoreceptors. *J. Neurosci.*, **17**, 8118–8128.
5. Boon, C.J., den Hollander, A.I., Hoyng, C.B., Cremers, F.P., Klevering, B.J. and Keunen, J.E. (2008) The spectrum of retinal dystrophies caused by mutations in the peripherin/RDS gene. *Prog. Retin. Eye Res.*, **27**, 213–235.
6. Aleman, T.S., Lam, B.L., Cideciyan, A.V., Sumaroka, A., Windsor, E.A., Roman, A.J., Schwartz, S.B., Stone, E.M. and Jacobson, S.G. (2009) Genetic heterogeneity in autosomal dominant retinitis pigmentosa with low-frequency damped electroretinographic wavelets. *Eye (Lond.)*, **23**, 230–233.
7. Simonelli, F., Testa, F., Marini, V., Interlandi, E., Rossi, S., Pognuz, D.R., Virgili, G., Garre, C. and Bandello, F. (2007) Intrafamilial clinical heterogeneity associated with a novel mutation of the retinal degeneration slow/peripherin gene. *Ophthalmic Res.*, **39**, 255–259.
8. van Lith-Verhoeven, J.J., Cremers, F.P., van den Helm, B., Hoyng, C.B. and Deutman, A.F. (2003) Genetic heterogeneity of butterfly-shaped pigment dystrophy of the fovea. *Mol. Vis.*, **9**, 138–143.
9. Weigell-Weber, M., Kryenbuhl, C., Buchi, E.R. and Spiegel, R. (1996) Genetic heterogeneity in autosomal dominant pattern dystrophy of the retina. *Mol. Vis.*, **2**, 6.
10. Goldberg, A.F., Loewen, C.J. and Molday, R.S. (1998) Cysteine residues of photoreceptor peripherin/rds: role in subunit assembly and autosomal dominant retinitis pigmentosa. *Biochemistry*, **37**, 680–685.

11. Loewen, C.J. and Molday, R.S. (2000) Disulfide-mediated oligomerization of Peripherin/Rds and Rom-1 in photoreceptor disk membranes. Implications for photoreceptor outer segment morphogenesis and degeneration. *J. Biol. Chem.*, **275**, 5370–5378.
12. Goldberg, A.F. and Molday, R.S. (1996) Subunit composition of the peripherin/rds-rom-1 disk rim complex from rod photoreceptors: hydrodynamic evidence for a tetrameric quaternary structure. *Biochemistry*, **35**, 6144–6149.
13. Conley, S.M., Stuck, M.W., Watson, J.N., Zulliger, R., Burnett, J.L. and Naash, M.I. (2019) Prph2 initiates outer segment morphogenesis but maturation requires Prph2/Rom1 oligomerization. *Hum. Mol. Genet.*, **28**, 459–475.
14. Zulliger, R., Conley, S.M., Mwoyosvi, M.L., Al-Ubaidi, M.R. and Naash, M.I. (2018) Oligomerization of Prph2 and Rom1 is essential for photoreceptor outer segment formation. *Hum. Mol. Genet.*, **27**, 3507–3518.
15. Clarke, G., Goldberg, A.F., Vidgen, D., Collins, L., Ploder, L., Schwarz, L., Molday, L.L., Rossant, J., Szel, A., Molday, R.S., Birch, D.G. and McInnes, R.R. (2000) Rom-1 is required for rod photoreceptor viability and the regulation of disk morphogenesis. *Nat. Genet.*, **25**, 67–73.
16. Dryja, T.P., Hahn, L.B., Kajiwara, K. and Berson, E.L. (1997) Dominant and digenic mutations in the peripherin/RDS and ROM1 genes in retinitis pigmentosa. *Invest. Ophthalmol. Vis. Sci.*, **38**, 1972–1982.
17. Sullivan, L.S., Bowne, S.J., Birch, D.G., Hughbanks-Wheaton, D., Heckenlively, J.R., Lewis, R.A., Garcia, C.A., Ruiz, R.S., Blanton, S.H., Northrup, H. *et al.* (2006) Prevalence of disease-causing mutations in families with autosomal dominant retinitis pigmentosa: a screen of known genes in 200 families. *Invest. Ophthalmol. Vis. Sci.*, **47**, 3052–3064.
18. Kajiwara, K., Berson, E.L. and Dryja, T.P. (1994) Digenic retinitis pigmentosa due to mutations at the unlinked peripherin/RDS and ROM1 loci. *Science*, **264**, 1604–1608.
19. Kedzierski, W., Nusinowitz, S., Birch, D., Clarke, G., McInnes, R.R., Bok, D. and Travis, G.H. (2001) Deficiency of rds/peripherin causes photoreceptor death in mouse models of digenic and dominant retinitis pigmentosa. *Proc. Natl. Acad. Sci. USA.*, **98**, 7718–7723.
20. Poloschek, C.M., Bach, M., Lagreze, W.A., Glaus, E., Lemke, J.R., Berger, W. and Neidhardt, J. (2010) ABCA4 and ROM1: implications for modification of the PRPH2-associated macular dystrophy phenotype. *Invest. Ophthalmol. Vis. Sci.*, **51**, 4253–4265.
21. Rodriguez-Munoz, A., Aller, E., Jaijo, T., Gonzalez-Garcia, E., Cabrera-Peset, A., Gallego-Pinazo, R., Udaondo, P., Salom, D., Garcia-Garcia, G. and Millan, J.M. (2020) Expanding the clinical and molecular heterogeneity of nonsyndromic inherited retinal dystrophies. *J. Mol. Diagn.*, **22**, 532–543.
22. Stuck, M.W., Conley, S.M. and Naash, M.I. (2014) The Y141C knockin mutation in RDS leads to complex phenotypes in the mouse. *Hum. Mol. Genet.*, **23**, 6260–6274.
23. Conley, S.M., Stuck, M.W., Watson, J.N. and Naash, M.I. (2017) Rom1 converts Y141C-Prph2-associated pattern dystrophy to retinitis pigmentosa. *Hum. Mol. Genet.*, **26**, 509–518.
24. Vaclavik, V., Tran, H.V., Gaillard, M.C., Schorderet, D.F. and Munier, F.L. (2012) Pattern dystrophy with high intrafamilial variability associated with Y141C mutation in the peripherin/RDS gene and successful treatment of subfoveal CNV related to multifocal pattern type with anti-VEGF (ranibizumab) intravitreal injections. *Retina*, **32**, 1942–1949.
25. Chakraborty, D., Conley, S.M., Zulliger, R. and Naash, M.I. (2016) The K153Del PRPH2 mutation differentially impacts photoreceptor structure and function. *Hum. Mol. Genet.*, **25**, 3500–3514.
26. Chakraborty, D., Strayve, D.G., Makia, M.S., Conley, S.M., Kakahel, M., Al-Ubaidi, M.R. and Naash, M.I. (2020) Novel molecular mechanisms for Prph2-associated pattern dystrophy. *FASEB J.*, **34**, 1211–1230.
27. Conley, S.M., Stuck, M.W., Burnett, J.L., Chakraborty, D., Azadi, S., Fliesler, S.J. and Naash, M.I. (2014) Insights into the mechanisms of macular degeneration associated with the R172W mutation in RDS. *Hum. Mol. Genet.*, **23**, 3102–3114.
28. Ding, X.Q., Nour, M., Ritter, L.M., Goldberg, A.F., Fliesler, S.J. and Naash, M.I. (2004) The R172W mutation in peripherin/rds causes a cone-rod dystrophy in transgenic mice. *Hum. Mol. Genet.*, **13**, 2075–2087.
29. Weleber, R.G., Carr, R.E., Murphey, W.H., Sheffield, V.C. and Stone, E.M. (1993) Phenotypic variation including retinitis pigmentosa, pattern dystrophy, and fundus flavimaculatus in a single family with a deletion of codon 153 or 154 of the peripherin/RDS gene. *Arch. Ophthalmol.*, **111**, 1531–1542.
30. Fossarello, M., Bertini, C., Galantuomo, M.S., Cao, A., Serra, A. and Pirastu, M. (1996) Deletion in the peripherin/RDS gene in two unrelated Sardinian families with autosomal dominant butterfly-shaped macular dystrophy. *Arch. Ophthalmol.*, **114**, 448–456.
31. Kajiwara, K., Hahn, L.B., Mukai, S., Travis, G.H., Berson, E.L. and Dryja, T.P. (1991) Mutations in the human retinal degeneration slow gene in autosomal dominant retinitis pigmentosa. *Nature*, **354**, 480–483.
32. Zhang, K., Garibaldi, D.C., Li, Y., Green, W.R. and Zack, D.J. (2002) Butterfly-shaped pattern dystrophy: a genetic, clinical, and histopathological report. *Arch. Ophthalmol.*, **120**, 485–490.
33. Nakazawa, M., Wada, Y. and Tamai, M. (1995) Macular dystrophy associated with monogenic Arg172Trp mutation of the peripherin/RDS gene in a Japanese family. *Retina*, **15**, 518–523.
34. Wickham, L., Chen, F.K., Lewis, G.P., Uppal, G.S., Neveu, M.M., Wright, G.A., Robson, A.G., Webster, A.R., Grierson, I., Hiscott, P. *et al.* (2009) Clinicopathological case series of four patients with inherited macular disease. *Invest. Ophthalmol. Vis. Sci.*, **50**, 3553–3561.
35. Conley, S., Nour, M., Fliesler, S.J. and Naash, M.I. (2007) Late-onset cone photoreceptor degeneration induced by R172W mutation in Rds and partial rescue by gene supplementation. *Invest. Ophthalmol. Vis. Sci.*, **48**, 5397–5407.
36. Ding, X.Q., Stricker, H.M. and Naash, M.I. (2005) Role of the second intradiscal loop of peripherin/rds in homo and hetero associations. *Biochemistry*, **44**, 4897–4904.
37. Loewen, C.J., Moritz, O.L., Tam, B.M., Papermaster, D.S. and Molday, R.S. (2003) The role of subunit assembly in peripherin-2 targeting to rod photoreceptor disk membranes and retinitis pigmentosa. *Mol. Biol. Cell*, **14**, 3400–3413.
38. Chakraborty, D., Ding, X.Q., Conley, S.M., Fliesler, S.J. and Naash, M.I. (2009) Differential requirements for retinal degeneration slow intermolecular disulfide-linked oligomerization in rods versus cones. *Hum. Mol. Genet.*, **18**, 797–808.
39. Goldberg, A.F. and Molday, R.S. (2000) Expression and characterization of peripherin/rds-rom-1 complexes and mutants implicated in retinal degenerative diseases. *Methods Enzymol.*, **316**, 671–687.

40. Chakraborty, D., Conley, S.M., Nash, Z., Ding, X.Q. and Naash, M.I. (2012) Overexpression of ROM-1 in the cone-dominant retina. *Adv. Exp. Med. Biol.*, **723**, 633–639.
41. Farjo, R., Fliesler, S.J. and Naash, M.I. (2007) Effect of Rds abundance on cone outer segment morphogenesis, photoreceptor gene expression, and outer limiting membrane integrity. *J. Comp. Neurol.*, **504**, 619–630.
42. Chakraborty, D., Conley, S.M., Al-Ubaidi, M.R. and Naash, M.I. (2014) Initiation of rod outer segment disc formation requires RDS. *PLoS One*, **9**, e98939.
43. Conley, S.M., Al-Ubaidi, M.R., Han, Z. and Naash, M.I. (2014) Rim formation is not a prerequisite for distribution of cone photoreceptor outer segment proteins. *FASEB J.*, **28**, 3468–3479.
44. Tian, G., Ropelewski, P., Nemet, I., Lee, R., Lodowski, K.H. and Imanishi, Y. (2014) An unconventional secretory pathway mediates the cilia targeting of peripherin/rds. *J. Neurosci.*, **34**, 992–1006.
45. Zulliger, R., Conley, S.M., Mwoyosvi, M.L., Stuck, M.W., Azadi, S. and Naash, M.I. (2015) SNAREs interact with retinal degeneration slow and rod outer segment membrane Protein-1 during conventional and unconventional outer segment targeting. *PLoS One*, **10**, e0138508.
46. Nour, M., Ding, X.Q., Stricker, H., Fliesler, S.J. and Naash, M.I. (2004) Modulating expression of peripherin/rds in transgenic mice: critical levels and the effect of overexpression. *Invest. Ophthalmol. Vis. Sci.*, **45**, 2514–2521.
47. Nour, M., Fliesler, S.J. and Naash, M.I. (2008) Genetic supplementation of RDS alleviates a loss-of-function phenotype in C214S model of retinitis pigmentosa. *Adv. Exp. Med. Biol.*, **613**, 129–138.
48. Ali, R.R., Sarra, G.M., Stephens, C., Alwis, M.D., Bainbridge, J.W., Munro, P.M., Fauser, S., Reichel, M.B., Kinnon, C., Hunt, D.M., Bhattacharya, S.S. and Thrasher, A.J. (2000) Restoration of photoreceptor ultrastructure and function in retinal degeneration slow mice by gene therapy. *Nat. Genet.*, **25**, 306–310.
49. Cai, X., Conley, S.M., Nash, Z., Fliesler, S.J., Cooper, M.J. and Naash, M.I. (2010) Gene delivery to mitotic and postmitotic photoreceptors via compacted DNA nanoparticles results in improved phenotype in a mouse model of retinitis pigmentosa. *FASEB J.*, **24**, 1178–1191.
50. Cai, X., Nash, Z., Conley, S.M., Fliesler, S.J., Cooper, M.J. and Naash, M.I. (2009) A partial structural and functional rescue of a retinitis pigmentosa model with compacted DNA nanoparticles. *PLoS One*, **4**, e5290.
51. Petrs-Silva, H., Yasumura, D., Matthes, M.T., LaVail, M.M., Lewin, A.S. and Hauswirth, W.W. (2012) Suppression of rds expression by siRNA and gene replacement strategies for gene therapy using rAAV vector. *Adv. Exp. Med. Biol.*, **723**, 215–223.
52. Georgiadis, A., Tschernutter, M., Bainbridge, J.W., Robbie, S.J., McIntosh, J., Nathwani, A.C., Smith, A.J. and Ali, R.R. (2010) AAV-mediated knockdown of peripherin-2 in vivo using miRNA-based hairpins. *Gene Ther.*, **17**, 486–493.
53. Karczewski, K.J., Francioli, L.C., Tiao, G., Cummings, B.B., Alfoldi, J., Wang, Q., Collins, R.L., Laricchia, K.M., Ganna, A., Birnbaum, D.P. *et al.* (2020) The mutational constraint spectrum quantified from variation in 141,456 humans. *Nature*, **581**, 434–443.
54. Farjo, R., Skaggs, J.S., Nagel, B.A., Quiambao, A.B., Nash, Z.A., Fliesler, S.J. and Naash, M.I. (2006) Retention of function without normal disc morphogenesis occurs in cone but not rod photoreceptors. *J. Cell Biol.*, **173**, 59–68.
55. Chakraborty, D., Ding, X.Q., Fliesler, S.J. and Naash, M.I. (2008) Outer segment oligomerization of Rds: evidence from mouse models and subcellular fractionation. *Biochemistry*, **47**, 1144–1156.